The Journal of Immunology

Structural Insights into the Substrate Specificity of Human Granzyme H: The Functional Roles of a Novel RKR Motif

Li Wang, Kai Zhang, Lianfeng Wu, Shengwu Liu, Honglian Zhang, Qiangjun Zhou, Liang Tong, Fei Sun and Zusen Fan

J Immunol 2012; 188:765-773; Prepublished online 9 December 2011;
doi: 10.4049/jimmunol.1101381
http://www.jimmunol.org/content/188/2/765

The Journal of Immunology is published twice each month by
The American Association of Immunologists, Inc.,
9650 Rockville Pike, Bethesda, MD 20814-3994.

Print ISSN: 0022-1767 Online ISSN: 1550-6606.

Structural Insights into the Substrate Specificity of Human Granzyme H: The Functional Roles of a Novel RKR Motif

Li Wang,* Kai Zhang,† Lianfeng Wu,* Shengwu Liu,* Honglian Zhang,* Qiangjun Zhou,† Liang Tong,‡ Fei Sun,†,[1] and Zusen Fan*,[1]

Human granzyme H (GzmH) is constitutively expressed in human NK cells that have important roles in innate immune responses against tumors and viruses. GzmH is a chymotrypsin-like serine protease. Its substrate preference and its mechanism of substrate recognition are poorly understood. To provide structural insights into the substrate recognition mechanisms for GzmH, we solved the crystal structures of a D102N-GzmH mutant alone and in complex with a decapeptide substrate and an inhibitor to 2.2 Å, 2.4 Å, and 2.7 Å, respectively. The Thr^{189}, Gly^{216}, and Gly^{226} specificity triad in the S1 pocket of GzmH defines its preference for bulky, aromatic residues (Tyr and Phe) at the P1 position. Notably, we discovered that an unusual RKR motif (Arg^{39}-Lys^{40}-Arg^{41}), conserved only in GzmH, helps define the S3′ and S4′ binding regions, indicating the preference for acidic residues at the P3′ and P4′ sites. Disruption of the RKR motif or the acidic P3′ and P4′ residues in the substrate abolished the proteolytic activity of GzmH. We designed a tetrapeptide chloromethylketone inhibitor, Ac-PTSY-chloromethylketone, which can selectively and efficiently block the enzymatic and cytotoxic activity of GzmH, providing a useful tool for further studies on the function of GzmH. ***The Journal of Immunology*****, 2012, 188: 765–773.**

Natural killer cells and CTLs provide a powerful defense against transformed cells and virus-infected cells. Involved in this defense are major toxic molecules, such as perforin and the granzymes (Gzms), which are expressed by these cells (1–3). To date, five human Gzms have been identified. Not all their functions have been clearly defined (4–7). They differ from each other in their specificities for substrates, and therefore they probably execute cell death through different pathways (8). Their substrate specificity is probably caused by differences in the structures of the different granzymes. The crystal structures of four of the human Gzms, GzmA, B, K, and M, have been solved and have provided structural bases for understanding their choice of substrates (9–13).

Human GzmH gene belongs to the GzmB gene cluster on human chromosome 14. GzmH has 71% amino acid sequence identity with GzmB (14). GzmH is a chymotrypsin-like chymase and is capable of cleaving proteins at sites that contain bulky aromatic amino acids such as Tyr and Phe (15). Fellows et al. (16) showed that GzmH induces an alternative caspase-independent cell death without identified substrates. We previously showed that GzmH induces caspase-dependent apoptosis with DNA fragmentation through cleavage of inhibitor of caspase-activated DNase (ICAD) to release caspase-activated DNase (17), a reactivity that is reminiscent of that of GzmB. However, GzmB is an Aspase that cuts after Asp residues, based on its positively charged substrate-binding pocket (10). However, no structural study has yet precisely elucidated the structural criteria that determine the substrate specificity of GzmH.

Nevertheless, the substrate specificity of GzmH is of interest. GzmH is mainly expressed in human resting NK cells (16–18), which suggests that GzmH may play a critical role in innate immunity induced by NK cells. A previous report showed that GzmH exhibits antiviral activity by destroying the functions of important viral proteins such as the adenovirus DNA-binding protein for viral DNA replication and the adenovirus 100K assembly protein for virus assembly (19). The adenovirus 100K assembly protein is an inhibitor of GzmB. Thus, destruction of this viral protein by GzmH inhibits viral growth not only because of direct effects on the 100K protein, but also because this destruction allows the preservation of GzmB activity (19, 20). GzmH also degrades a multifunctional phosphoprotein La to inhibit hepatitis C virus-internal ribosome entry site-mediated translational activity (21). In this study, we solved the crystal structures of a D102N-GzmH variant alone and in complex with a decapeptide substrate and an inhibitor at 2.2 Å, 2.4 Å, and 2.7 Å, respectively. We identified the factors that determine the specificity of GzmH and an unusual RKR motif in its S′ binding region. The positively charged S′ region contributes to the specificity of the enzyme. We also designed a specific inhibitor that efficiently blocks the catalytic and cytotoxic activity of GzmH.

*Chinese Academy of Sciences Key Laboratory of Infection and Immunity, Institute of Biophysics, Chinese Academy of Sciences, Beijing 100101, China; †National Laboratory of Biomacromolecules, Institute of Biophysics, Chinese Academy of Sciences, Beijing 100101, China; and ‡Department of Biological Sciences, Columbia University, New York, NY 10027

[1]F.S. and Z.F. contributed equally to this work.

Received for publication May 11, 2011. Accepted for publication November 9, 2011.

This work was supported by the National Natural Science Foundation of China (30830030, 31128003, 31170837, 31021062, 30972676), the 973 Program (2010CB911902), and the Innovative Program of the Chinese Academy of Sciences (XDA01010407, KSCX1-YW-22).

The atomic coordinates and structure factors presented in this article have been submitted to the Protein Data Bank (http://www.rcsb.org) under ID codes 3TK9, 3TJV, and 3TJU.

Address correspondence and reprint requests to Dr. Fei Sun and Dr. Zusen Fan, Institute of Biophysics, Chinese Academy of Sciences, 15 Datun Road, Beijing 100101, China. E-mail addresses: feisun@ibp.ac.cn (F.S.) and fanz@moon.ibp.ac.cn (Z.F.)

The online version of this article contains supplemental material.

Abbreviations used in this article: CMA, concanamycin A; CMK, chloromethylketone; Gzm, granzyme; ICAD, inhibitor of caspase-activated DNase; PI, propidium iodide; rICAD, recombinant ICAD; rLA, recombinant LA; SLO, streptolysin O; wt, wild type.

Materials and Methods

Cell lines, Abs, and reagents

YTS cells and the MHC class I-negative mutant B lymphoblastoid cell line 721.221 cells (provided by B. Ge, Institute of Health Science, Chinese Academy of Sciences, Shanghai, China) were maintained in RPMI 1640 medium supplemented with 10% FBS, 100 U/ml penicillin, and 100 μg/ml streptomycin. Commercial Abs were β-actin (BD Pharmingen), rabbit antiserum against NM23-H1 (Santa Cruz Biotechnology), and rabbit polyclonal Ab against La (Abcam). Rabbit antiserum against ICAD was provided by R.P. Sekaly (Laboratoire d'Immunologie, Universite´ de Montreal, Montreal, QC, Canada). Mouse mAb against GzmH (Abcam) is specific for GzmH and does not cross-react with other Gzms (data not shown). Concanamycin A (CMA) was from Sigma-Aldrich.

Protein expression and purification

All the constructs were generated by the standard PCR-based cloning strategies and verified by sequencing. Mutagenesis was performed by Stratagene QuikChange site-directed mutagenesis kit. Human GzmH and its mutants were cloned into vector pET28a with an additional N-terminal enterokinase cleavage sequence (DDDDK). The proteins were overexpressed in *Escherichia coli* Rosetta (DE3) as inclusion bodies and then refolded, as previously described (13, 16). After removal of a 6×His tag and redundant residues at N terminus by enterokinase (Novagen), intact GzmH was further purified by HighTrap S Sepharose chromatography (GE Healthcare). Full-length human La protein and ICAD were cloned into pET28a and pET26b separately, expressed as soluble proteins in *E. coli* Rosetta (DE3), and purified, as previously reported (17, 22).

Crystallization and data collection

Initial crystallization screening was carried out with commercially available sparse matrix screens (Hampton Research). Crystals were generated in 2 μl hanging drops containing equal amounts of protein (8–10 mg/ml) and mother liquor equilibrated over 200 μl reservoir solution at 16˚C. D102N-GzmH was crystallized in a buffer containing 0.2 M Li_2SO_4, 0.1 M Bicine (pH 8.5), and 25% (w/v) PEG3350 after 1-wk incubation. For the generation of D102N-GzmH-decapeptide and D102N-GzmH–inhibitor complexes, crystals of D102N-GzmH were soaked in the above mother liquor supplemented with either 10 mM decapeptide for 2 d or 2 mM inhibitor for 18 h. For data collection, crystals were dehydrated in a solution containing 0.2 M Li_2SO_4, 0.1 M Bicine (pH 8.5), and 30% (w/v) PEG3350 for 2 h and then fast frozen with liquid nitrogen. All data sets were collected at −173˚C. Data for D102N-GzmH, D102N-GzmH-decapeptide, and D102N-GzmH-inhibitor complexes were respectively collected at the beamline BL6A (λ = 1.0 Å), BL17A (λ = 0.98 Å), and NE3A (λ = 1.0 Å) of Photon Factory. All diffraction data were indexed, integrated, and scaled with the program HKL2000 (23). Data collection statistics are summarized in Table I.

Structure determination and refinement

The initial structure of D102N-GzmH was solved by molecular replacement with PHASER (24) using human GzmB as a search model (Protein Data Bank accession code 1IAU) (10). The structure of D102N-GzmH was then used as the search model for solving the structures of D102N-GzmH-decapeptide and D102N-GzmH-inhibitor complexes. All structure refinement was carried out with CNS (25) and REFMAC (26), and COOT was used for manual model building (27). A summary of refinement statistics is provided in Table I. Stereochemical parameters were evaluated with PROCHECK (28).

Enzymatic assay

Enzymatic activity of GzmH and its mutants was measured by coincubation of 0.3 μM enzyme with 300 μM (if not otherwise mentioned) synthetic substrate Ac-PTSY-pNA at 25˚C in 25 mM Tris (pH 8.0) and 150 mM NaCl, monitoring the absorbance at 405 nM with a Multilable Counter (Wallac 1420 Victor; PerkinElmer). For inhibition analysis, various Gzms were preincubated for 1 h at 37˚C with or without the inhibitor and then assayed for residual activity with corresponding substrate, as follows: Suc-VANR-pNA for GzmA, Z-IEPD-AFC for GzmB, Ac-YRFK-pNA for GzmK, and Suc-AAPL-pNA for GzmM.

Cleavage assay

K562 cell lysates (10^5 total cells) were incubated with active GzmH at 37˚C for 2 h in 20 μl cleavage buffer containing 25 mM Tris (pH 8.0), 150 mM NaCl, 1 mM $CaCl_2$, and 1 mM $MgCl_2$, as described (29). For recombinant protein cleavage assay, recombinant LA (rLA) or recombinant ICAD (rICAD) was treated with equal amounts of GzmH and its variants at 37˚C for 20 min. All reactions were terminated by 5× loading buffer, resolved by SDS-PAGE, and probed by Commassie blue staining or immunoblotting.

Loading GzmH with streptolysin O

GzmH was loaded into Jurkat cells with 80 ng/ml streptolysin O (SLO; Sigma-Aldrich), as described (30). Briefly, SLO was preactivated by 10 mM DTT for 10 min. Jurkat cells (2×10^5) were treated with 0.5 μM GzmH plus the indicated concentrations of the Ac-PTSY-chloromethylketone (CMK) at 37˚C for 7 h. Then cells were harvested and stained with FITC-conjugated annexin V and propidium iodide (PI; Bender MedSystems), followed by flow cytometry (FACSCalibur; BD Biosciences). Data were analyzed by FlowJo software (Tree Star).

[^{51}Cr] release assay

YTS killer cells were maintained in RPMI 1640 media supplemented with 10% FCS (Life Technologies). The human EBV-transformed B cell line 721.221 as target cells were labeled with 200 μCi [^{51}Cr] and plated at 10^4 cells/well at 37˚C for 1 h. YTS cells were incubated with the target cells at the indicated E:T ratios for an additional 4 h incubation, as described (31). For inhibition assay, YTS cells were pretreated with 500 nM CMA for 2 h or with 600 nM GzmH inhibitor for 1 h before incubation with target cells. Specific cytotoxicity was calculated as follows: ([sample release − spontaneous release]/[total release − spontaneous release]) × 100%.

Detection of the second order rate constants

The second order constant (k_i) was conducted to analyze the specificity of Ac-PTSY-CMK inhibitor. Human cathepsin G and neutrophil elastase were purchased from Calbiochem, and the mast cell chymase was from Sigma-Aldrich. Peptidyl substrates (Ac-FLF-pNA, Ac-AAPL-pNA, Ac-PTSY-pNA) were synthesized by Beijing Scilight Biotechnology. Generally, aliquots (30 nM each) of each protein were mixed with or without the Ac-PTSY-CMK inhibitor at various time intervals (from 0 to 180 min), prior to the addition of 0.3 mM substrates. Residual activity was measured by Multilable Counter (Wallac 1420 Victor; PerkinElmer) at 405 nm. The pseudo-first order rate constants (k1) were calculated by the negative slope from the plot of LN (V_t/V_0) versus inhibition time. V_t represents the remaining activity of pretreated enzyme, and V_0 represents the remaining activity of untreated control. The second order rate constant (k_i) was calculated through dividing k1 by the concentration of the inhibitor.

Results

Overall structure of human GzmH

Our recent study revealed that Asp[102] and His[57] in the catalytic triad are critical for the hydrolytic activity of Gzms (chymotrypsinogen numbering is used throughout) (13). The D102N mutants of GzmM and GzmA completely lost their catalytic activity. In addition, we found that D102N-GzmH is more stable and homogeneous than wild type (wt) and S195A-GzmH (data not shown). Human recombinant GzmH and its variants were expressed as inclusion bodies and refolded, as described previously (13, 16). We have determined the crystal structures of GzmH (D102N mutant) alone (PDB code 3TK9) and in complex with a decapeptide substrate (PDB code 3TJV) and a designed inhibitor (PDB code 3TJU) at up to 2.2 Å resolutions (Table I).

The structure of D102N-GzmH is of high quality. Residues from the N-terminal Ile[16] to Leu[245] are all visible in the electron density map. It consists of 2 α-helices and 13 β-strands, assembled into two juxtaposed β-barrel domains that are bridged by the catalytic triad. The N-terminal residues insert into the cleft with strong internal salt bridge with Asp[194] to maintain the rigid structure and the substrate binding site. Three intramolecular disulfide bridges (Cys[42]-Cys[58], Cys[136]-Cys[201], and Cys[168]-Cys[182]) are well identified in the structure with a free Cys[166] protruding from α-helix1 into the solvent. The Cys[166] does not form an intermolecular disulfide bridge (data not shown). Thus, it is structurally unlikely for GzmH to form a homodimer. The secondary structure and sequence alignment of GzmH with other human Gzms are shown in Supplemental Fig. 1.

Table I. X-ray diffraction data collection and refinement statistics

GzmH Structure	D102N-GzmH	D102N-GzmH with Peptide	D102N-GzmH with Inhibitor
Data collection			
Space group	$P4_12_12$	$P4_12_12$	$P4_12_12$
Cell dimensions			
a, b, c (Å)	63.9, 63.9, 142.5	57.8, 57.8, 142.8	63.2, 63.2, 144.8
α, β, γ (°)	90, 90, 90	90, 90, 90	90, 90, 90
Resolution (Å)[a]	58.3-2.2 (2.3-2.2)	50-2.4 (2.5-2.4)	50-2.7 (2.8-2.7)
R_{merge}[a, b]	0.064 (0.315)	0.080 (0.317)	0.099 (0.248)
I/σ(I)[a]	27.6 (3.3)	30.2 (3.4)	58.5 (12.7)
Completeness (%)[a]	99.4 (98.6)	98.8 (92.9)	99.4 (99.6)
Redundancy[a]	9.1 (6.0)	29.4 (12.3)	35.5 (22.2)
Wilson plot B factor	35.2	38.1	50.6
Refinement			
Resolution (Å)	50-2.2	50-2.4	50-2.7
No. reflections	14,758	9,482	8,604
R_{work}/R_{free}[c]	0.251/0.277	0.234/0.243	0.229/0.288
No. atoms			
Protein	1,769	1,761	1,760
Peptide		64	
Inhibitor			36
Ligand/ion	5	10	15
Water	41	22	30
B factors			
Protein	43.6	20.5	34.4
Peptide		27.9	
Inhibitor			38.4
Ligand/ion	45.4	70.0	63.5
Water	41.8	18.1	33.9
Total	43.5	21.0	34.8
R.M.S. deviations			
Bond length (Å)	0.015	0.012	0.015
Bond angles (°)	1.8	1.3	1.6
Ramachandran plot			
Most favored (%)	82.1	83.1	83.2
Additionally allowed (%)	16.8	16.4	16.2
Generously allowed (%)	1.0	0.5	1.0
Disallowed	0	0	0

[a]Highest resolution shell statistics are shown in parentheses.
[b]R_{merge} is defined by $R_{merge} = \Sigma_h\Sigma_i | I_{ih} - <I_h> |/\Sigma_h\Sigma_i < I_h>$, where $< I_h>$ is the mean of the observations I_{ih} of reflection h.
[c]R_{work} is defined by $R_{work} = \Sigma(||F_p(obs)| - |F_p(calc)||)/ \Sigma|F_p$ (obs)|; R_{free} = R factor for a selected subset (5%) of the reflections that was not included in prior refinement calculations.

Based on structural analysis and previous peptide substrate screening (32), we designed a decapeptide substrate PTSYAGDDSG that covers the P4 to P6′ residues and obtained the structure of the complex at 2.4 Å resolution (Fig. 1*B*). The decapeptide substrate snugly docks onto the crevice sandwiched by the two β-barrel domains, running perpendicularly to the catalytic triad (Fig. 1*B*, *left panel*). All the residues of the peptide exhibited continuous density, with the exception of C-terminal Gly at the P6′ site, which thus was not present in the structure (Fig. 1*B*, *right panel*). The detailed interactions between D102N-GzmH and the peptide substrate are depicted in Supplemental Fig. 2. Notably, the substrate-binding avenue is composed of two distinct halves, one half containing hydrophobic S pockets, and the other with positively charged S′ binding region. The structure therefore suggests that GzmH prefers hydrophobic residues at the N terminus and acidic residues C-terminal to the scissile bond.

Preference of bulky aromatic residues at P1 position

To elucidate the hydrophobic preference for bulky residues, we first depicted the binding mode of the substrate with GzmH at the S pocket. The residues involved in the extensive interactions are shown in Fig. 2*A*. The S1 site [P and S nomenclature, as described (33)] of GzmH functions as a major determinant and is assembled by loop 189 (183–196) and loop 220 (215–226). The specificity triad composed of three residues at positions of 189, 216, and 226 in the two loops makes the most contribution. Variations at any of the three residues can result in a fundamental change in substrate specificity (34). Human GzmH has a Thr^{189}, Gly^{216}, and Gly^{226} triad, whereas GzmB harbors Thr^{189}, Gly^{216}, and Arg^{226} (Fig. 2*B*, *left panel*). Orientated by a *cis* Pro^{224}-Pro^{225} motif, Arg^{226} in GzmB points into the binding pocket and recognizes negatively charged Asp or Glu P1 residue in the substrate for proteolysis. In contrast to GzmB, Gly^{226} in GzmH enlarges the S1 site without any change of electrostatic property of the pocket, and so readily accommodates large residues such as Tyr and Phe (Fig. 2*B*, *right panel*). To test the role of Gly^{226}, we made Gly to Arg-substituted GzmH (G226R-GzmH). We tested the enzymatic activities of wt GzmH and G226R-GzmH toward both the tetra-peptidyl substrate (Ac-PTSY-pNA) and the substrate Ac-Tyr-pNA (Ac-Y-pNA). Even with high concentrations of G226R-GzmH (1.2 μM), G226R-GzmH failed to hydrolyze both synthetic substrates Ac-PTSY-pNA and Ac-Y-pNA (Fig. 2*C*, *left panel*). In contrast, wt GzmH efficiently hydrolyzed the substrate Ac-PTSY-pNA in a time-dependent manner, whereas wt GzmH showed no catalytic activity against the substrate Ac-Tyr-pNA within 2 h. However, with longer incubation, wt GzmH was able to cleave the Ac-Tyr-pNA substrate after 24 h. In contrast, G226R-GzmH still had no catalytic activity even after 48 h with the same substrate Ac-Tyr-pNA (Fig. 2*C*, *right panel*). Moreover, G226R-GzmH cleaved neither rICAD and rLa proteins nor their native forms of K562 cell lysates (Fig. 2*D*). By contrast, wt GzmH

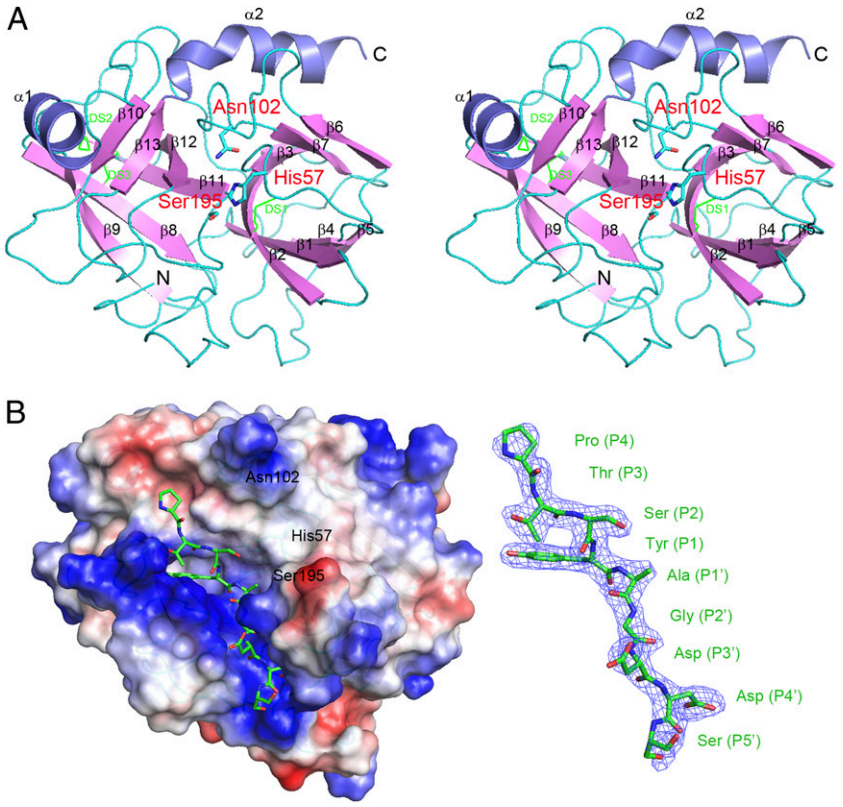

FIGURE 1. Overall structures of human GzmH alone and in complex with a decapeptide substrate. *A*, A stereo representation of the structure of human GzmH (D102N mutant) in standard orientation (10). The active site residues (His[57], Asp[102]Asn, and Ser[195]) are rendered as stick models (nitrogen atoms, blue; oxygen atoms, red), and the side chains of the three disulfides (DS1, Cys[42]-Cys[58]; DS2, Cys[168]-Cys[182]; DS3, Cys[136]-Cys[201]) of GzmH are shown as lines in green. The β-strands, loops, and helices are colored violet, cyan, and blue, respectively. The N and C termini are labeled "N" and "C," respectively. All the ribbon figures in this article were prepared with PyMOL (http://www.pymol.org/), if not otherwise stated. *B*, The electrostatic surface view of GzmH in complex with a decapeptide substrate. The bound decapeptide (PTSYAGDDSG) is shown in a green stick representation. The orientation is the same as in *A*. Experimental electron density ($2F_o$-F_c map) at 2.4 Å resolution for the peptide is shown in blue in the *right panel*, contoured at 1.0 σ. The last Gly residue of the peptide is not shown due to lack of density.

processed these two substrates in both recombinant and native forms. NM23H1 was unchanged as a loading control. Taken together, Gly[226] plays a critical role in substrate binding for GzmH.

As for concrete interactions at S1 site, we found that the carbonyl group of Tyr at P1 position is well stabilized by oxyanion hole formed by Gly[193], Asp[194], and Ser[195]. The hydroxyphenyl ring of Tyr accounts for the major hydrophobic interactions with Phe[191], Tyr[215], and the carbon atoms of Gly[216] and Lys[192] (Fig. 2*A*). Particularly, Phe[191] displays the same conformation irrespective of substrate-binding status, which is quite different from that in GzmC, where Phe[191] fills up the S1 pocket and blocks activity (35). GzmH maintains an open S1 pocket to accommodate the substrate. Additionally, the hydroxyl group of Tyr is hydrogen bonded to the carbonyl group of Asn[217], which may explain the preference for Tyr over Phe and Met in the library screening results (32).

An unusual RKR motif forms the unique positive binding site of the S′ sites

Our structure shows that a RKR motif plays an important role in recognizing acidic P′ residues, a feature that is unique to GzmH (Fig. 3*A*, Supplemental Fig. 3). The motif is composed of residues Arg[39], Lys[40], and Arg[41], located on the β2-strand, whose backbones form the wall of S4′ site. The side chains of Arg[39], Arg[41], Gln[34], and Lys[74] complete the S4′ site (Fig. 3*B*). Compared with GzmB, a register shift of loop 37 (36A-38) in GzmH orients the RKR motif closer to the binding cleft to hydrogen bond with the substrate (Fig. 3*C*). The P4′ Asp is rigidly sequestered by the RKR motif. Oδ1 atom of P4′ Asp forms a salt bridge with Nη2 atom of Arg[41], whereas Oδ2 atom interacts with Nη2 group of Gln[34]. Additional interaction lies in the main chain hydrogen bonds and hydrophobic interactions between carbon atoms.

The structure of the complex also reveals an additional role of the RKR motif at S3′ site. The side chain of Lys[40] interacts with Asp at P3′ position through a salt bridge. Superposition of GzmB with GzmH suggests that Lys[40] in GzmB could interact with the P3′ residues rather than P4′ residue, as previously deduced (36) (Fig. 3*C*).

To confirm the structural observations for the importance of the RKR motif in recognizing acidic P′ residues, we mutated the P3′ and P4′ Asp residues in the La protein substrate of GzmH. Mutations of P3′ and P4′ Asp residues in La protein completely disrupted GzmH-mediated hydrolysis, which is consistent with a previous report (21). Taken together, the RKR motif defines preference for acidic residues in P3′ and P4′ sites for GzmH. RKR motif in GzmH is highly conserved in placental mammals (Fig. 3*D*). Furthermore, RKR motif only exists in GzmH. These suggest that RKR motif exerts a unique role in substrate recognition for GzmH.

The S′ positive binding region restricts recognition specificity of physiological substrates

The cocrystal structure reveals the mechanism of specific requirement for acidic residues at P3′ and P4′ sites. To address prevalence of this preference for acidic residues, we first identified the cleavage site in a previously reported physiological substrate ICAD (17). Based on sequence analysis, the 108-QESFDVDETD-117 sequence in ICAD is consistent with the requirement for acidic residues at P3′ and P4′ sites. As expected, Phe[111]Val-ICAD mutant was not cleaved by GzmH (Fig. 4*A*). Another sequence 213-KAAFGEEVDA-222 in ICAD is partially congruent with the requirement. Interestingly, Phe[216]Val-ICAD mutant was weakly proteolyzed by GzmH in vitro, but was not a substrate in vivo. The sequence 361-KTKFASDDEH-370 in La adheres to the structural basis for acidic residues at P3′ and P4′ sites (21) (Fig. 4*A*), which is a recognition sequence for cleavage by GzmH. To further verify the acidic requirement of S′ binding region, we mutated the P3′ and P4′ residues of ICAD to generate a D114A-E115A-ICAD (DE-AA-ICAD) mutant. We found that GzmH did not cleave DE-AA-ICAD either (Fig. 4*B*).

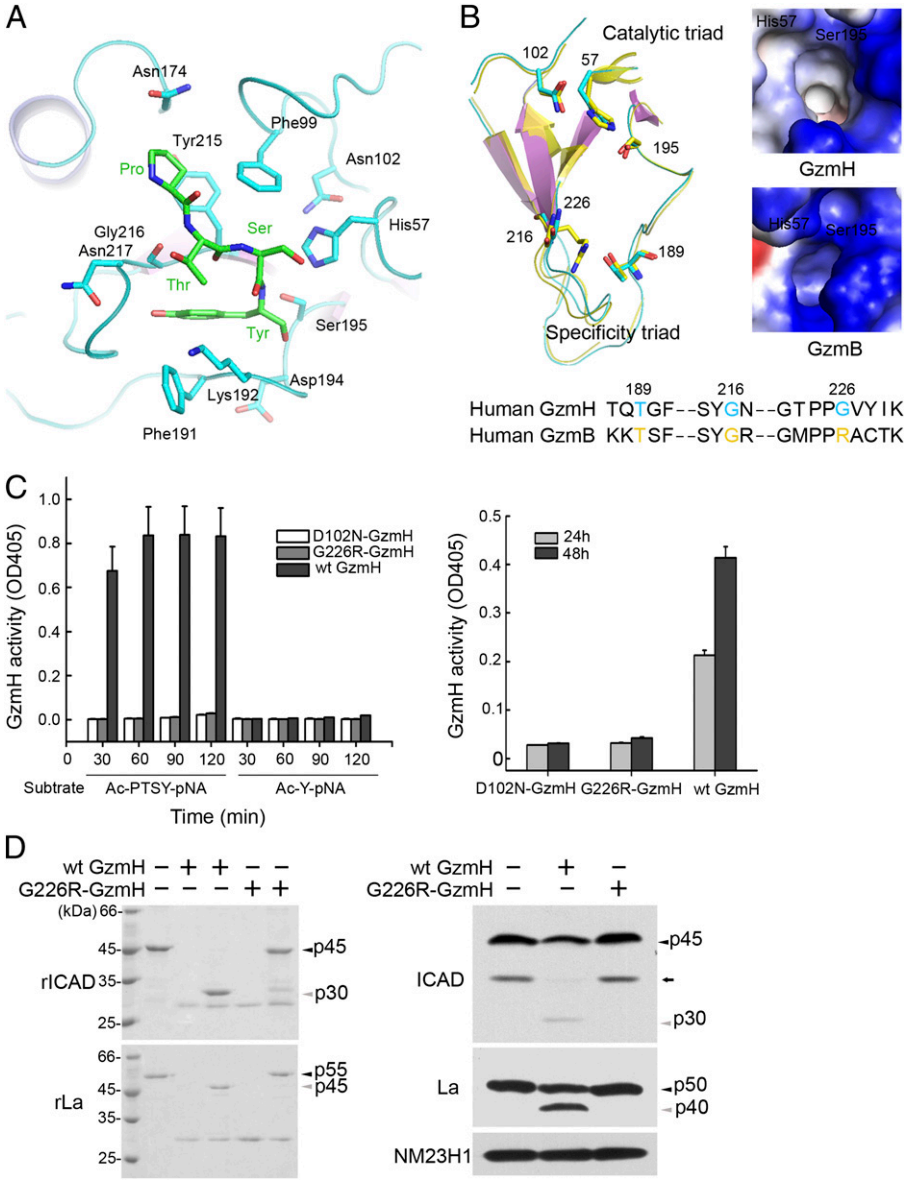

FIGURE 2. Interactions between GzmH and the substrate decapeptide. *A*, The S pockets of GzmH nicely accommodate the P1 to P4 residues. Key interaction residues are shown as sticks in cyan. *B*, Alignments of the structure and sequence of GzmH (cyan) and GzmB (yellow, from 1IAU) (10) at the specificity triad. Residues at 189, 216, and 226 sites determine the P1 specificity in chymotrypsin-like serine protease family. GzmH and GzmB share the same Thr^{189} and Gly^{216} architecture, differing at 226. Arg^{226} in GzmB contributes to its Aspase activity and the positively charged property of the S1 pocket, whereas Gly^{226} in GzmH enlarges the binding pocket and maintains the hydrophobic environment, conferring the aromatic specificity. For clarity, this figure was drawn by a 90° counterclockwise rotation from the standard orientation. *C*, Gly^{226}Arg-substituted GzmH (G226R-GzmH) completely loses the chymotrypsin-like activity. G226R-GzmH (1.2 μM) and wt GzmH (1.2 μM) were incubated with either Ac-PTSY-pNA or Ac-Y-pNA (1.2 mM) at 37°C for the indicated times, followed by absorbance detection at 405 nM (*left panel*). The enzymatic activities were measured after 24 and 48 h for the hydrolysis of Ac-Y-pNA substrate. D102N-GzmH serves as a catalytically inactive control. These data are representative of three independent experiments and shown as mean ± SD. *D*, G226R-GzmH is inactive toward physiological substrates of GzmH. rICAD and rLa proteins were treated with wt GzmH or G226R-GzmH at 37°C for 12 min and visualized by Coomassie brilliant blue staining (*left panel*). K562 cell lysates were incubated with equal amounts of wt GzmH or G226R-GzmH at 37°C for 2 h, followed by immunoblotting. The same blot was stripped for probing of NM23H1. A short isoform of ICAD is labeled by an arrow mark.

To determine the direct impact of the S′ binding region on catalysis, we constructed a series of GzmH mutants, with changes in the S′ positive binding region, including R41L-GzmH, K40A-GzmH, K74A-GzmH, R39A-R41L-GzmH (RR-AL-GzmH), R39A-K40A-R41L-GzmH (RKR-AAL-GzmH), and K74A-R39A-R41L-GzmH (KRR-AAL-GzmH). Because none of the mutations involves the catalytic triad and the substrate-binding pockets for the tetrapeptide substrate, all the mutants except RKR-AAL-GzmH showed similar enzymatic activities for cleavage of this tetrapeptide substrate (Fig. 4*C*). We also analyzed the kinetic constants of all the GzmH mutants, as shown in the Supplemental Table I. All the GzmH variants, except RKR-AAL-GzmH, exhibited similar enzymatic constants to hydrolyze the Ac-PTSY-pNA substrate. However, the RKR-AAL-GzmH mutant showed 4-fold higher K_m value and 10-fold lower k_{cat} value than other mutants. The RKR-AAL-GzmH mutation abolished enzymatic activity, which may have disrupted the β_2-strand, leading to collapse of rigid structure.

We next assessed whether S′ site mutations influence degradation of physiological substrates. We expressed rICAD and rLa proteins and incubated them with GzmH in vitro. wt GzmH could completely cleave rICAD and rLa (Fig. 4*D*). However, these two substrates were resistant to the GzmHs carrying double or triple mutations (RR-AL-GzmH, RKR-AAL-GzmH, and KRR-AAL-GzmH). In comparison, GzmHs carrying a single mutation were able to degrade half of each substrate, exhibiting reduced activity compared with wt GzmH. Similar results were obtained through loading experiments to ascertain the enzyme-induced cell death, as previously reported (4) (data not shown).

A selective inhibitor for GzmH

Given that the N-terminal residues PTSY of decapeptide substrate nicely fit in the catalytic site, we hypothesized that it could be a foundation for designing a specific inhibitor. Therefore, we designed a compound with acetylated-Pro at P4 and CMK-linked Tyr at P1. The crystal structure of GzmH bound to this inhibitor was determined at 2.7 Å resolution (Table I, Fig. 5*A*). The structure confirms that the Ac-PTSY-CMK compound is an irreversible inhibitor that blocks GzmH through snugly docking into the active site and cross-linking with Ser^{195}-OH and His^{57}-Nε2 atoms.

The Ac-PTSY-CMK compound completely blocked enzymatic activity in a dose- and time-dependent manner assayed by proteolysis of the tetrapeptide substrate (Fig. 5*B*, 5*C*). The compound

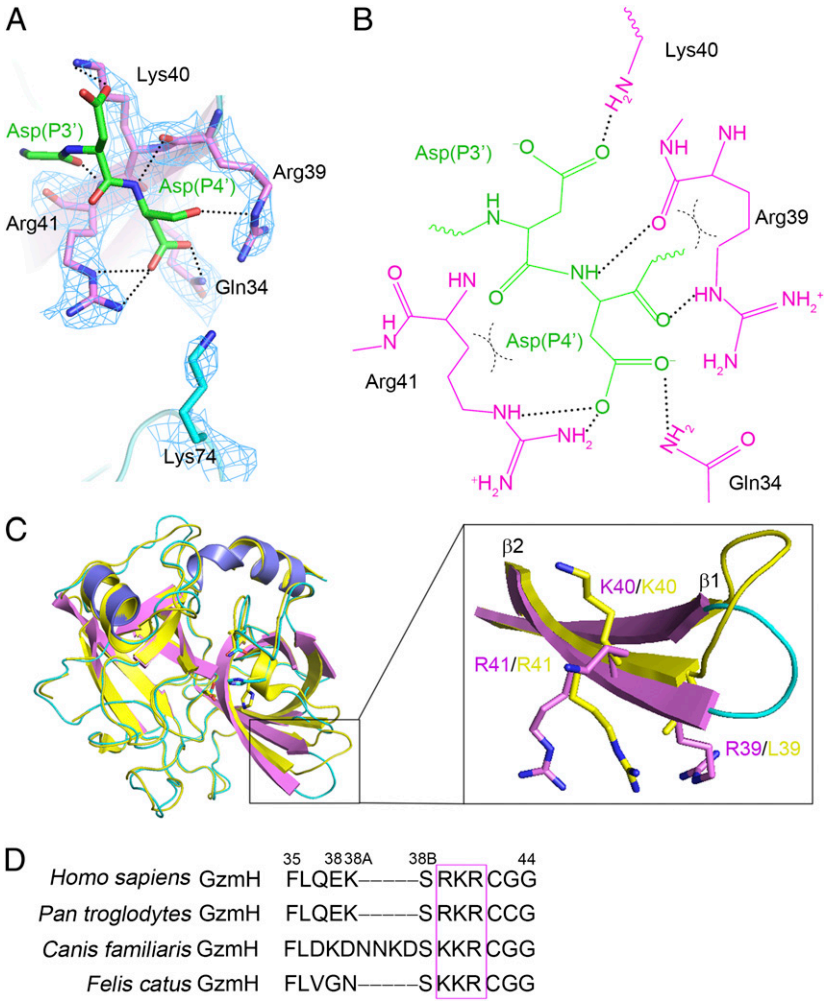

FIGURE 3. RKR motif in the S′ binding site forms a positive patch that recognizes acidic P′ residues. *A*, A detailed view of RKR motif. Residues of GzmH are colored in violet, and the $2F_o$-F_c electron density in blue mesh. The P3′ and P4′ substrate residues are in green. *B*, Schematic drawing of RKR motif elements for substrate recognition. Hydrogen bonds are denoted as black dashed lines, and hydrophobic interactions by dashed curves. *C*, Superimposition of overall structure of GzmB (yellow) to GzmH and a closer view of the RKR motif in the black frame, which suggests conformational differences at this site between the two enzymes. *D*, Alignment of the amino acids of GzmH in different species. Residue numbers are according to chymotrypsin numbering. RKR triplets are highlighted in a violet box.

also blocked the cleavage of the physiological substrates ICAD and La in K562 tumor cell lysates (Fig. 5*D*), whereas NM23H1 was not cleaved as a control. We next tested the specificity of this inhibitor by incubation of the compound with all five human Gzms. As shown in Fig. 5*E*, the Ac-PTSY-CMK inhibitor only inhibited enzymatic activity of GzmH, and had no activity on other Gzms. To further determine the specificity of the Ac-PTSY-CMK inhibitor toward GzmH, we synthesized the substrates for cathepsin G (Ac-FLF-pNA), neutrophil elastase (Ac-AAPL-pNA), and chymase (Ac-FLF-pNA) and analyzed the second order rate constants (k_i). The inhibitor Ac-PTSY-CMK had no inhibitory effect on the neutrophil elastase. The Ac-PTSY-CMK inhibitor exhibited much more efficient inhibitory effects on GzmH than the human chymase and the human cathepsin G. Their second order inhibition rate constants were 0.081 ± 0.012 μM^{-1} min^{-1}, 4.97 ± 0.93 μM^{-1} min^{-1}, and 0.59 ± 0.014 μM^{-1} min^{-1}, respectively.

We compared several delivery agents to load Gzms into target cells, including perforin, SLO, and a cationic lipid protein transfection agent Pro-Ject (6, 30). We found SLO efficiently delivered Gzms into target cells to induce cytolysis with similar kinetics of perforin delivery, which is in agreement with a previous report (16). Therefore, we used a low dose of SLO (80 ng/ml) to deliver GzmH into Jurkat cells to determine the inhibitory action of the GzmH inhibitor Ac-PTSY-CMK. We found that the Ac-PTSY-CMK inhibitor could repress GzmH-induced cell death (Fig. 5*F*). Over 8-fold excess of the GzmH, the Ac-PTSY-CMK inhibitor almost blocked enzymatic activity of GzmH. GzmH plays an important role in NK cell-mediated cytolysis against viruses and tumors (16, 17, 19, 21). Thus, we determined the effect of the inhibitor on NK cell-mediated cytotoxicity. NK cell line YTS cells, which express GzmH (Fig. 5*G*, *right panel*), were pretreated with the inhibitor prior to incubation with ^{51}Cr-labeled target 721.221 cells. The inhibitor strikingly suppressed YTS cell-mediated cell death (Fig. 5*G*, *left panel*). CMA, an inhibitor of cytotoxic granule exocytosis, could block YTS cell-mediated cytolysis as a positive control. Taken together, the Ac-PTSY-CMK compound is a selective and efficient inhibitor for human GzmH.

Discussion

GzmH is quite unique among all Gzms for its unusual role against tumors and viruses through degradation of its specific physiological substrates and essential viral proteins (16, 17, 19–21). However, little is known about how GzmH initiates viral clearance and cell apoptosis. In this study, our crystal structures have revealed detailed substrate specificity determinants for human GzmH. We found that Gly^{226} accounts for the primary restriction of bulky aromatic residues in P1 site and that a special RKR motif determines the recognition of P′ acidic residues. The hydrophobic S pockets and positively charged S′ binding region confine the recognition of physiological substrates.

Notably, our structure shows that an RKR motif, situated in the β_2-strand, is a major determinant of the S′ binding region. The pattern of triple basic residues is only conserved in GzmH of different species, suggesting that a similar mechanism may be adopted by GzmHs to recognize their physiological substrates. GzmB, the closest homolog for GzmH, only has Lys^{40} and Arg^{41}, but with

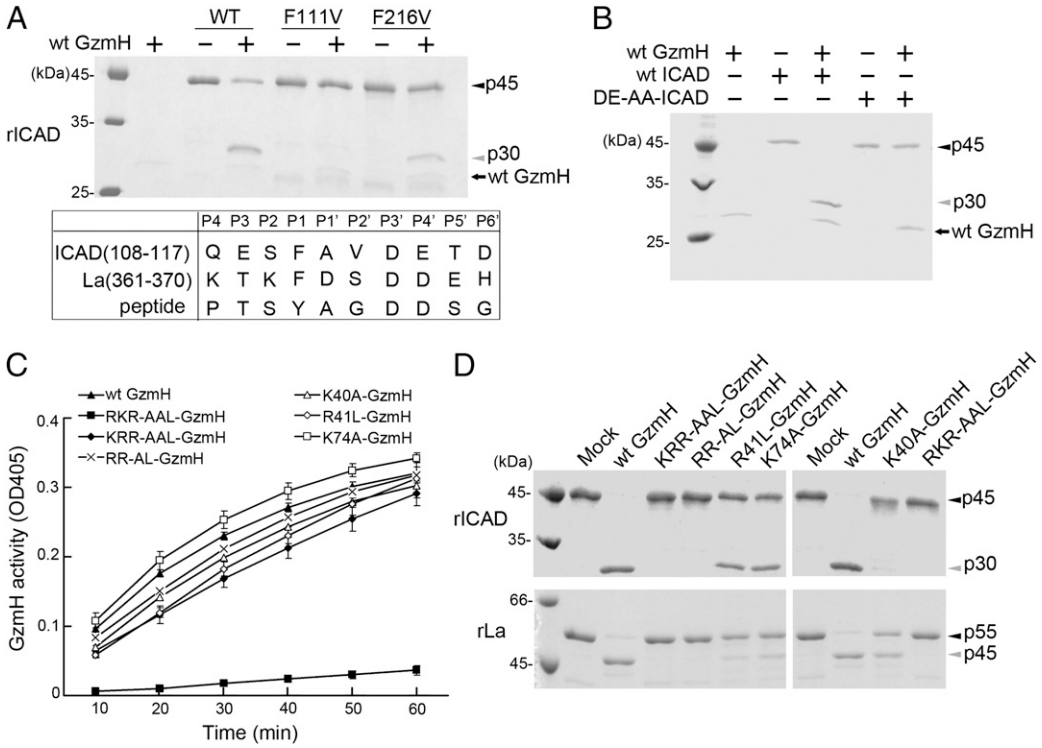

FIGURE 4. GzmH harbors restricted substrate specificity determined by the S′ positive region. *A*, The cleavage site was identified for ICAD. F111V-mutated ICAD completely abrogates the GzmH degradation. F111V, Phe^{111}Val-ICAD; F216V, Phe^{216}Val-ICAD. *B*, GzmH fails to cleave an ICAD mutant D114A-E115A-ICAD (DE-AA-ICAD). DE-AA-ICAD was generated by mutation of the P3′ and P4′ acidic residues of ICAD. DE-AA-ICAD and wt ICAD were treated with wt GzmH, followed by Coomassie brilliant blue staining. *C*, Enzymatic activities of GzmH and its mutants (0.3 μM) were detected by hydrolysis of Ac-PTSY-pNA substrate (0.3 mM). All GzmH mutants were expressed and purified using the same protocol as for wt GzmH. Data represent three independent experiments and are shown as mean ± SD. *D*, Proteolytic activity for GzmH and its mutants was confirmed by cleavage of physiological substrates. Human rLa and rICAD were treated with equal amount of the indicated GzmHs and separated by SDS-PAGE, followed by Coomassie brilliant blue staining.

Leu^{39}. Lys^{40} of GzmB was suggested to make a salt bridge with P4′ Glu (36). Cathepsin G, sharing 57% identity with GzmH, harbors Gln^{39}, Ser^{40}, and Arg^{41}, and may have a salt bridge between Arg^{41} and an acidic residue at position P2′ or P3′ (37). In this study, we found that Lys^{40} forms a salt bridge with Asp at P3′ position. Lys^{40} to Ala mutation made no change to hydrolyze the tetrapeptide substrate, while reducing proteolytic activity to physiological substrates. Our finding is in accordance with previous studies (36), implying a possible mechanism that disruption of Lys^{40}-P3′ salt bridge reduces the binding affinity and leads to decreased cleavage events. The P4′ Asp indeed interacts with the whole RKR motif by strong hydrogen bonds. Gln^{34} and Arg^{41} rigidly anchor the carboxyl group of P4′ Asp, and Arg^{41} attracts the main chain carbonyl and amide groups. A recent study demonstrated that physiological substrate La lacking P′ positive residues became insensitive to GzmH cleavage (21). Similarly, disruption of the whole RKR motif in GzmH abolished enzymatic activity and cleavage of physiological substrates, suggesting the RKR motif plays an essential role in maintaining molecular stability and substrate recognition. A recent study on insect chymotrypsin also implied the important binding contact at this region (38).

Although most of the Gzms follow a similar procedure to enter the target cells assisted by perforin, recognize and cleave substrates, and finally lead to cell death, they discriminate from each other by distinct binding machinery to different substrates, and thus execute cell death through different pathways (8). This discrimination could be attributed to structural variances that determine their specificities even though they adopt structurally canonical chymotrypsin-like serine protease architecture (Supplemental Fig. 3). GzmA and GzmK share a common Asp^{189} at the bottom of the catalytic site, giving rise to a tryptase-like activity with electrostatically complementary recognition of P1 residues as Arg and Lys (11, 12). However, it has been reported that GzmA and GzmK display a highly restricted profile of substrate specificities that partially overlap, suggesting the existence of other structural determinants (39). For GzmB, Arg^{226} renders its Aspase activity akin to caspases with specific binding of Asp and Glu (9, 10). Our study on GzmM showed that GzmM has a preference for long narrow hydrophobic amino acids as Met and Leu that are restricted by the size and hydrophobic properties of the binding site (13). In this study, we found that Gly^{226} in GzmH enlarges the S1 pocket and accommodates large residues such as Tyr and Phe at the P1 site.

No murine GzmH has been identified, and therefore a GzmH knockout mouse model for antiviral and antitumor investigation in vivo is not available. Chemical inhibition of human GzmH is an important alternative for studying the physiological roles of this enzyme. However, currently available inhibitors for GzmH are not specific (15), which hinders further research for GzmH functions. In this study, we developed a tetrapeptide inhibitor Ac-PTSY-CMK that completely blocked enzymatic activity and cleavage of physiological substrate by GzmH as well as attenuated NK cell-mediated cytotoxicity. This inhibitor selectively blocked catalytic activity for GzmH, but had no effect on other Gzms and neutrophil elastase. Because Gzms have functional redundancy, specific inhibitors are required for the functional study of a single member of the Gzm family. Granule killer-mediated cytolysis has been linked to allograft rejection and autoimmune diseases (40). Spe-

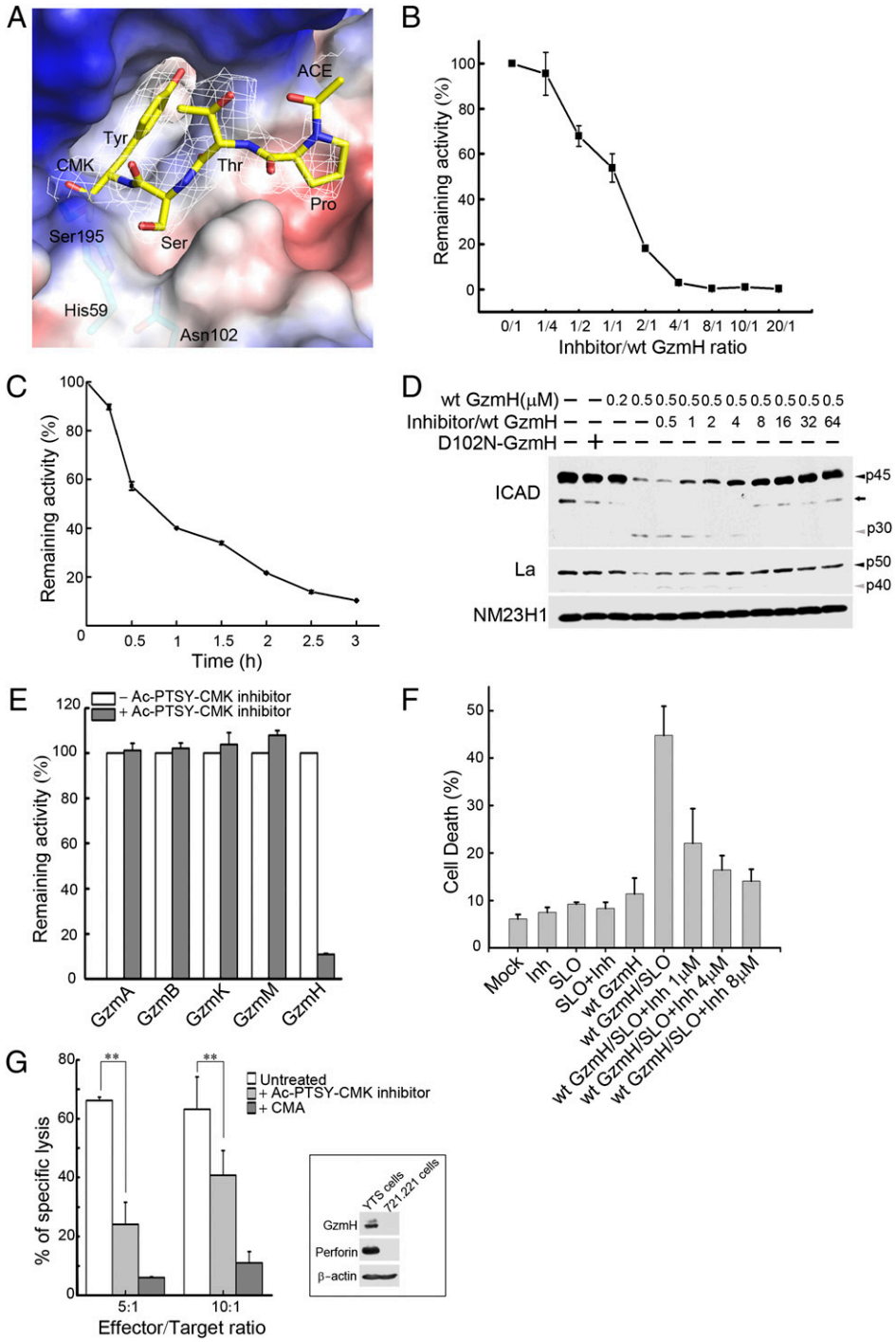

FIGURE 5. A specific inhibitor for GzmH. *A*, Schematic drawing showing the binding of the Ac-PTSY-CMK inhibitor to the active site of GzmH. The inhibitor is depicted as stick models in yellow. The CMK group is covalently linked to Ser^{195} and His^{57}. σ_A-weighted $2F_o$-F_c electron density map of the inhibitor is shown as the mesh in white, contoured at 1σ. ACE, acetyl group. *B* and *C*, The inhibitor efficiently blocks catalytic activity of GzmH in a dose (*B*)- and time (*C*)-dependent manner. wt GzmH (0.3 μM) was preincubated with different concentrations of the Ac-PTSY-CMK inhibitor (0 nM, 75 nM, 150 nM, 300 nM, 600 nM, 1.2 μM, 2.4 μM, 4.8 μM, and 6 μM) at 37°C for 0.5 h (*B*) or with equal molar of the inhibitor (0.3 μM) for the indicated times and followed by detecting enzymatic activity. *D*, The Ac-PTSY-CMK inhibitor abrogates degradation of physiological substrates of GzmH. K562 cell lysates were treated with different [inhibitor]/[enzyme] and probed for native ICAD and La. The corresponding concentrations of the inhibitor were 0 μM, 0.25 μM, 0.5 μM, 1 μM, 2 μM, 4 μM, 8 μM, 16 μM, and 32 μM, consistent with the indicated [inhibitor]/[enzyme] molar ratios (0.5–64). NM23H1 was used as a loading control. A short isoform of ICAD is labeled by an arrow mark. *E*, The Ac-PTSY-CMK inhibitor is specific for GzmH. All five human Gzms were pretreated or untreated with the inhibitor for 1 h, respectively. Residual activities were tested at 405 nm after 0.5-h incubation with the corresponding substrate at 37°C. Remaining enzymatic activity of individual Gzms was compared with that without inhibitor treatment. *F*, GzmH inhibitor Ac-PTSY-CMK can block cell death in GzmH-loaded intact cells. Jurkat cells were loaded with GzmH plus subdose of SLO (80 ng/ml) and stained with FITC-annexin V and PI, followed by flow cytometry. Percentage of dead cells was calculated with FITC-annexin V and PI double-positive cells by using FlowJo software. Data are representative of at least three independent experiments shown as mean ± SD. Inh, GzmH inhibitor Ac-PTSY-CMK. *G*, The inhibitor blocks NK cell-mediated cytotoxicity. NK cell line YTS cells were cultured with or without the Ac-PTSY-CMK compound (0.6 μM) for 1 h prior to incubation with its target 721.221 cells in different E/T ratios. After 4-h killing, percentage of specific lysis was analyzed by standard [^{51}Cr] release assay. YTS cells pretreated with 500 nM CMA were used as a positive control (*right panel*). Data represent three independent experiments and are shown as mean ± SD. $^{**}p < 0.01$. Expression of GzmH and perforin in YTS cells was assessed by immunoblotting (*right panel*). β-actin was used as a loading control.

cific inhibitors to block NK cell-mediated cytotoxicity may be a potential approach for organ transplantation or autoimmune disorders (41–43).

Acknowledgments

We thank Dr. Baoxue Ge for providing YTS and 721.221 cell lines and Dr. R.P. Sekaly for providing the Ab for ICAD. We thank Drs. Philippa Marrack and John Kappler for assistance and English editing. We also thank Dr. Yujia Zhai, Xiaoyun Pang, Jun Ma, and Yingzhi Xu for assistance with crystallization and data collection. We thank Shuo Wang and Haidong Tang for helpful discussion.

Disclosures

The authors have no financial conflicts of interest.

References

1. Chowdhury, D., and J. Lieberman. 2008. Death by a thousand cuts: granzyme pathways of programmed cell death. *Annu. Rev. Immunol.* 26: 389–420.
2. Trapani, J. A., and M. J. Smyth. 2002. Functional significance of the perforin/granzyme cell death pathway. *Nat. Rev. Immunol.* 2: 735–747.
3. Fan, Z., and Q. Zhang. 2005. Molecular mechanisms of lymphocyte-mediated cytotoxicity. *Cell. Mol. Immunol.* 2: 259–264.
4. Hu, D., S. Liu, L. Shi, C. Li, L. Wu, and Z. Fan. 2010. Cleavage of survivin by granzyme M triggers degradation of the survivin-X-linked inhibitor of apoptosis protein (XIAP) complex to free caspase activity leading to cytolysis of target tumor cells. *J. Biol. Chem.* 285: 18326–18335.
5. Hua, G., S. Wang, C. Zhong, P. Xue, and Z. Fan. 2009. Ignition of p53 bomb sensitizes tumor cells to granzyme K-mediated cytolysis. *J. Immunol.* 182: 2152–2159.
6. Zhao, T., H. Zhang, Y. Guo, Q. Zhang, G. Hua, H. Lu, Q. Hou, H. Liu, and Z. Fan. 2007. Granzyme K cleaves the nucleosome assembly protein SET to induce single-stranded DNA nicks of target cells. *Cell Death Differ.* 14: 489–499.
7. Hua, G., Q. Zhang, and Z. Fan. 2007. Heat shock protein 75 (TRAP1) antagonizes reactive oxygen species generation and protects cells from granzyme M-mediated apoptosis. *J. Biol. Chem.* 282: 20553–20560.
8. Cullen, S. P., and S. J. Martin. 2008. Mechanisms of granule-dependent killing. *Cell Death Differ.* 15: 251–262.
9. Waugh, S. M., J. L. Harris, R. Fletterick, and C. S. Craik. 2000. The structure of the pro-apoptotic protease granzyme B reveals the molecular determinants of its specificity. *Nat. Struct. Biol.* 7: 762–765.
10. Rotonda, J., M. Garcia-Calvo, H. G. Bull, W. M. Geissler, B. M. McKeever, C. A. Willoughby, N. A. Thornberry, and J. W. Becker. 2001. The three-dimensional structure of human granzyme B compared to caspase-3, key mediators of cell death with cleavage specificity for aspartic acid in P1. *Chem. Biol.* 8: 357–368.
11. Hink-Schauer, C., E. Estébanez-Perpiñá, E. Wilharm, P. Fuentes-Prior, W. Klinkert, W. Bode, and D. E. Jenne. 2002. The 2.2-A crystal structure of human pro-granzyme K reveals a rigid zymogen with unusual features. *J. Biol. Chem.* 277: 50923–50933.
12. Bell, J. K., D. H. Goetz, S. Mahrus, J. L. Harris, R. J. Fletterick, and C. S. Craik. 2003. The oligomeric structure of human granzyme A is a determinant of its extended substrate specificity. *Nat. Struct. Biol.* 10: 527–534.
13. Wu, L., L. Wang, G. Hua, K. Liu, X. Yang, Y. Zhai, M. Bartlam, F. Sun, and Z. Fan. 2009. Structural basis for proteolytic specificity of the human apoptosis-inducing granzyme M. *J. Immunol.* 183: 421–429.
14. Grossman, W. J., P. A. Revell, Z. H. Lu, H. Johnson, A. J. Bredemeyer, and T. J. Ley. 2003. The orphan granzymes of humans and mice. *Curr. Opin. Immunol.* 15: 544–552.
15. Edwards, K. M., C. M. Kam, J. C. Powers, and J. A. Trapani. 1999. The human cytotoxic T cell granule serine protease granzyme H has chymotrypsin-like (chymase) activity and is taken up into cytoplasmic vesicles reminiscent of granzyme B-containing endosomes. *J. Biol. Chem.* 274: 30468–30473.
16. Fellows, E., S. Gil-Parrado, D. E. Jenne, and F. C. Kurschus. 2007. Natural killer cell-derived human granzyme H induces an alternative, caspase-independent cell-death program. *Blood* 110: 544–552.
17. Hou, Q., T. Zhao, H. Zhang, H. Lu, Q. Zhang, L. Sun, and Z. Fan. 2008. Granzyme H induces apoptosis of target tumor cells characterized by DNA fragmentation and Bid-dependent mitochondrial damage. *Mol. Immunol.* 45: 1044–1055.
18. Sedelies, K. A., T. J. Sayers, K. M. Edwards, W. Chen, D. G. Pellicci, D. I. Godfrey, and J. A. Trapani. 2004. Discordant regulation of granzyme H and granzyme B expression in human lymphocytes. *J. Biol. Chem.* 279: 26581–26587.
19. Andrade, F., E. Fellows, D. E. Jenne, A. Rosen, and C. S. Young. 2007. Granzyme H destroys the function of critical adenoviral proteins required for viral DNA replication and granzyme B inhibition. *EMBO J.* 26: 2148–2157.
20. Waterhouse, N. J., and J. A. Trapani. 2007. H is for helper: granzyme H helps granzyme B kill adenovirus-infected cells. *Trends Immunol.* 28: 373–375.
21. Romero, V., E. Fellows, D. E. Jenne, and F. Andrade. 2009. Cleavage of La protein by granzyme H induces cytoplasmic translocation and interferes with La-mediated HCV-IRES translational activity. *Cell Death Differ.* 16: 340–348.
22. Jacks, A., J. Babon, G. Kelly, I. Manolaridis, P. D. Cary, S. Curry, and M. R. Conte. 2003. Structure of the C-terminal domain of human La protein reveals a novel RNA recognition motif coupled to a helical nuclear retention element. *Structure* 11: 833–843.
23. Otwinowski, Z., and W. Minor. 1997. Processing of X-ray diffraction data collected in oscillation mode. In *Macromolecular Crystallography, Part A, Methods in Enzymology*, Vol. 276. C. W. Carter, Jr. and R. M. Sweet, eds. Academic Press, New York, p. 307–326.
24. Read, R. J. 2001. Pushing the boundaries of molecular replacement with maximum likelihood. *Acta Crystallogr. D Biol. Crystallogr.* 57: 1373–1382.
25. Brunger, A. T. 2007. Version 1.2 of the crystallography and NMR system. *Nat. Protoc.* 2: 2728–2733.
26. Murshudov, G. N., A. A. Vagin, and E. J. Dodson. 1997. Refinement of macromolecular structures by the maximum-likelihood method. *Acta Crystallogr. D Biol. Crystallogr.* 53: 240–255.
27. Emsley, P., and K. Cowtan. 2004. Coot: model-building tools for molecular graphics. *Acta Crystallogr. D Biol. Crystallogr.* 60: 2126–2132.
28. Laskowski, R. A., J. A. Rullmannn, M. W. MacArthur, R. Kaptein, and J. M. Thornton. 1996. AQUA and PROCHECK-NMR: programs for checking the quality of protein structures solved by NMR. *J. Biomol. NMR* 8: 477–486.
29. Fan, Z., P. J. Beresford, D. Y. Oh, D. Zhang, and J. Lieberman. 2003. Tumor suppressor NM23-H1 is a granzyme A-activated DNase during CTL-mediated apoptosis, and the nucleosome assembly protein SET is its inhibitor. *Cell* 112: 659–672.
30. Shi, L., L. Wu, S. Wang, and Z. Fan. 2009. Granzyme F induces a novel death pathway characterized by Bid-independent cytochrome c release without caspase activation. *Cell Death Differ.* 16: 1694–1706.
31. Fan, Z., P. J. Beresford, D. Zhang, Z. Xu, C. D. Novina, A. Yoshida, Y. Pommier, and J. Lieberman. 2003. Cleaving the oxidative repair protein Ape1 enhances cell death mediated by granzyme A. *Nat. Immunol.* 4: 145–153.
32. Mahrus, S., and C. S. Craik. 2005. Selective chemical functional probes of granzymes A and B reveal granzyme B is a major effector of natural killer cell-mediated lysis of target cells. *Chem. Biol.* 12: 567–577.
33. Schechter, I., and A. Berger. 1967. On the size of the active site in proteases. I. Papain. *Biochem. Biophys. Res. Commun.* 27: 157–162.
34. Wouters, M. A., K. Liu, P. Riek, and A. Husain. 2003. A despecialization step underlying evolution of a family of serine proteases. *Mol. Cell* 12: 343–354.
35. Kaiserman, D., A. M. Buckle, P. Van Damme, J. A. Irving, R. H. Law, A. Y. Matthews, T. Bashtannyk-Puhalovich, C. Langendorf, P. Thompson, J. Vandekerckhove, et al. 2009. Structure of granzyme C reveals an unusual mechanism of protease autoinhibition. *Proc. Natl. Acad. Sci. USA* 106: 5587–5592.
36. Sun, J., J. C. Whisstock, P. Harriott, B. Walker, A. Novak, P. E. Thompson, A. I. Smith, and P. I. Bird. 2001. Importance of the P4′ residue in human granzyme B inhibitors and substrates revealed by scanning mutagenesis of the proteinase inhibitor 9 reactive center loop. *J. Biol. Chem.* 276: 15177–15184.
37. Korkmaz, B., T. Moreau, and F. Gauthier. 2008. Neutrophil elastase, proteinase 3 and cathepsin G: physicochemical properties, activity and physiopathological functions. *Biochimie* 90: 227–242.
38. Dunse, K. M., Q. Kaas, R. F. Guarino, P. A. Barton, D. J. Craik, and M. A. Anderson. 2010. Molecular basis for the resistance of an insect chymotrypsin to a potato type II proteinase inhibitor. *Proc. Natl. Acad. Sci. USA* 107: 15016–15021.
39. Bovenschen, N., R. Quadir, A. L. van den Berg, A. B. Brenkman, I. Vandenberghe, B. Devreese, J. Joore, and J. A. Kummer. 2009. Granzyme K displays highly restricted substrate specificity that only partially overlaps with granzyme A. *J. Biol. Chem.* 284: 3504–3512.
40. Li, B., C. Hartono, R. Ding, V. K. Sharma, R. Ramaswamy, B. Qian, D. Serur, J. Mouradian, J. E. Schwartz, and M. Suthanthiran. 2001. Noninvasive diagnosis of renal-allograft rejection by measurement of messenger RNA for perforin and granzyme B in urine. *N. Engl. J. Med.* 344: 947–954.
41. Gouet, P., E. Courcelle, D. I. Stuart, and F. Métoz. 1999. ESPript: analysis of multiple sequence alignments in PostScript. *Bioinformatics* 15: 305–308.
42. Wallace, A. C., R. A. Laskowski, and J. M. Thornton. 1995. LIGPLOT: a program to generate schematic diagrams of protein-ligand interactions. *Protein Eng.* 8: 127–134.
43. Lottenberg, R., and C. M. Jackson. 1983. Solution composition dependent variation in extinction coefficients for p-nitroaniline. *Biochim. Biophys. Acta* 742: 558–564.